Applied Mathematical Modelling 38 (2014) 1523–1533

Contents lists available at ScienceDirect

Applied Mathematical Modelling

journal homepage: www.elsevier.com/locate/apm

Non-linear oscillations of a thin-walled composite beam with shear deformation

Sebastián P. Machado *, C. Martín Saravia, Franco E. Dotti

Grupo Análisis de Sistemas Mecánicos, Centro de Investigaciones de Mecánica Teórica y Aplicada, Universidad Tecnológica Nacional FRBB, 11 de Abril 461, B8000LMI Bahía Blanca, Argentina
Consejo Nacional de Investigaciones Científicas y Tecnológicas, CONICET, Argentina

ARTICLE INFO

Article history:
Received 16 February 2012
Received in revised form 31 May 2013
Accepted 5 August 2013
Available online 27 August 2013

Keywords:
Shear flexibility
Internal resonance
Composite material
Thin-walled beams

ABSTRACT

A geometrically non-linear theory is used to study the dynamic behavior of a thin-walled composite beam. The model is based on a small strain and large rotation and displacements theory, which is formulated through the adoption of a higher-order displacement field and takes into account shear flexibility (bending and warping shear). In the analysis of a weakly nonlinear continuous system, the Ritz's method is employed to express the problem in terms of generalized coordinates. Then, perturbation method of multiple scales is applied to the reduced system in order to obtain the equations of amplitude and modulation. In this paper, the non-linear 3D oscillations of a simply-supported beam are examined, considering a cross-section having one symmetry axis. Composite is assumed to be made of symmetric balanced laminates and especially orthotropic laminates. The model, which contains both quadratic and cubic non-linearities, is assumed to be in internal resonance condition. Steady-state solution and their stability are investigated by means of the eigenvalues of the Jacobian matrix. The equilibrium solution is governed by the modal coupling and experience a complex behavior composed by saddle noddle, Hopf and double period bifurcations.

1. Introduction

Thin-walled beam structures made of advanced anisotropic composite materials are increasingly found in the design of the aircraft wing, helicopter blade, axles of vehicles and so on, due to their outstanding engineering properties, such as high strength/stiffness to weight ratios and favorable fatigue characteristics. The interesting possibilities provided by fiber reinforced composite materials can be used to enhance the response characteristics of such structures that operate in complex environmental conditions. We consider the nonlinear response of a simply supported beam to a primary resonant excitation of its first mode. The analysis accounts for a lateral load, modal damping and two fiber orientations. The second and third natural frequencies are approximately two and three times the first natural frequency, respectively. The flexural–torsional coupling produces a quadratic and cubic nonlinearity in the governing nonlinear partial-differential equation. Because of the quadratic and cubic nonlinearity and the two-to-one and three-to-one ratio of the second and third with the first natural frequencies, the beam exhibits an internal (autoparametric) resonance that couples the first, second and third modes, resulting in energy exchange between them.

* Corresponding author at: Grupo Análisis de Sistemas Mecánicos, Centro de Investigaciones de Mecánica Teórica y Aplicada, Universidad Tecnológica Nacional FRBB, 11 de Abril 461, B8000LMI Bahía Blanca, Argentina. Tel.: +54 0291 4555220; fax: +54 0291 4555311.
E-mail address: smachado@frbb.utn.edu.ar (S.P. Machado).

0307-904X/$ - see front matter © 2013 Elsevier Inc. All rights reserved.
http://dx.doi.org/10.1016/j.apm.2013.08.028

For a comprehensive review of nonlinear modal interactions, we refer the reader to Refs. [1–3]. In this paper, we present a brief review of some of the studies of the response of systems exhibiting two-to-one and three-to-one internal resonances to primary resonant excitations.

Crespo da Silva and Glynn [4,5] developed a non-linear shear-undeformable beam model with a compact cross-section and derived a set of integro-partial-differential equations governing flexural–flexural–torsional motions of inextensional beams, including geometric and inertia nonlinearities. They used these equations and the method of multiple scales to ascertain the importance of the geometric terms [5]; they found that they cannot be neglected for the lower modes, especially the first mode. Luongo et al. [6] and Crespo da Silva and Zaretzky [7] analyzed shear and axially undeformable beams. In the last reference the flexural–torsional free motions are studied for a cantilever beam, having close bending and torsional frequencies; although beams with non-compact cross-section are considered, the warping effects are neglected. In these articles a non-linear one-dimensional polar model of compact beam is derived, capable of studying interactions between flexural and torsional motions occurring in beam-like structures in several internal resonance conditions. The non-linear planar motions and the non-linear resonance frequencies was recently investigated by Fonseca and Ribeiro [8]. They used a p-version finite element formulated for geometrically non-linear vibrations. Lopes Alonso and Ribeiro [9] continued this last work [8] for the free vibrations of clamped–clamped circular cross section beams using hierarchic sets of displacement shape functions and that simultaneously considers bending, torsion and longitudinal deformation. In this case, they employed the harmonic balance method to show the variation of the bending and torsional shapes of vibration with the non-linear natural frequency. The effects of the warping function, longitudinal displacements of second order and shear deformations on the nonlinear bending-torsion vibrations of rectangular cross section was analyzed in the work of Stoykov and Ribeiro [10]. In relation to thin-walled beams, Di Egidio et al. [11,12] presented the dynamic response of an open cross-section beam divided in two works. They developed a shear undeformable thin-walled beam where the effects of non linear in-plane and out-of-plane warping and torsional elongation were included in the model [11]. The dynamic coupling phenomena in conditions of internal resonance was analyzed in the second part [12]. Machado and Saravia [13] investigated the effect of shear deformation on the frequency–response curves of a thin-walled composite beam. They showed that the equilibrium solutions are influenced by the transverse shear effect. The amplitude of vibration is reduced significantly when this effect is ignored, altering the dynamic response of the beam.

In this paper, a geometrically non-linear beam model is used to study three dimensional large amplitude oscillations. It is shown that the system exhibits periodic and quasiperiodic responses for a typical range of parameter values. The limit cycles which born from the Hopf bifurcation are analyzed. A schematic bifurcation diagrams for the orbits of the modulation equations is presented. The mathematical model is valid for symmetric balanced laminates and incorporates, in a full form, the effects of shear flexibility. In order to perform the nonlinear dynamic analysis the Galerkin procedure is used to obtain a discrete form of the equations of motion. Multiple time scales method is used to obtain modulation-phase equations [14] and the reconstitution method proposed in [15] is adopted to return to the true time domain. Steady state solutions and their stability are studied by using the model proposed. For principal parametric resonance of the first mode, the influence of internal resonance is illustrated in frequency and amplitude plots.

2. Kinematics

A straight thin-walled composite beam with an arbitrary cross-section is considered (Fig. 1). The points of the structural member are referred to a Cartesian co-ordinate system $(x,\overline{y},\overline{z})$, where the x-axis is parallel to the longitudinal axis of the beam while $\overline{y}$ and $\overline{z}$ are the principal axes of the cross-section. The axes y and z are parallel to the principal ones but having their origin at the shear center (defined according to Vlasov's theory of isotropic beams). The co-ordinates corresponding to points lying on the middle line are denoted as Y and Z (or $\overline{y}$ and $\overline{z}$). In addition, a circumferential co-ordinate s and a normal co-ordinate n are introduced on the middle contour of the cross-section.

$$\overline{y}(s,n)=\overline{Y}(s)-n\frac{dZ}{ds},\quad \overline{z}(s,n)=\overline{Z}(s)+n\frac{dY}{ds}, \tag{1}$$

$$y(s,n)=Y(s)-n\frac{dZ}{ds},\quad z(s,n)=Z(s)+n\frac{dY}{ds}. \tag{2}$$

On the other hand, y_0 and z_0 are the centroidal co-ordinates measured with respect to the shear center.

$$\overline{y}(s,n)=y(s,n)-y_0,\quad \overline{z}(s,n)=z(s,n)-z_0. \tag{3}$$

The present structural model is based on the following assumptions [16]:

(1) The cross-section contour is rigid in its own plane.
(2) The warping distribution is assumed to be given by the Saint–Venant function for isotropic beams.
(3) Flexural rotations (about the $\overline{y}$ and $\overline{z}$ axes) are assumed to be moderate, while the twist ϕ of the cross-section can be arbitrarily large.
(4) Shell force and moment resultants corresponding to the circumferential stress σ_{ss} and the force resultant corresponding to γ_{ns} are neglected.

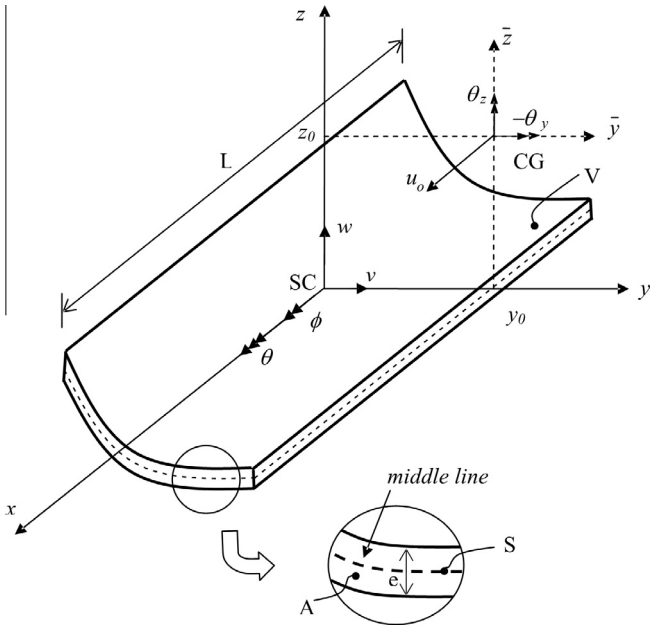

Fig. 1. Co-ordinate system of the cross-section and notation for displacement measures.

(5) The curvature at any point of the shell is neglected.
(6) Twisting linear curvature of the shell is expressed according to the classical plate theory.
(7) The laminate stacking sequence is assumed to be symmetric and balanced [17].

According to these hypotheses the displacement field is assumed to be in the following form

$$\begin{aligned} u_x &= u_o - \overline{y}(\theta_z\cos\phi - \theta_y\sin\phi) - \overline{z}(\theta_y\cos\phi - \theta_z\sin\phi) + \omega\left[\theta - \frac{1}{2}(\theta_y'\theta_z - \theta_y\theta_z')\right] + (\theta_z z_0 - \theta_y y_0)\sin\phi, \\ u_y &= v - z\sin\phi - y(1-\cos\phi) - \frac{1}{2}(\theta_z^2\overline{y} + \theta_z\theta_y\overline{z}), \\ u_z &= w + y\sin\phi - z(1-\cos\phi) - \frac{1}{2}(\theta_y^2\overline{z} + \theta_z\theta_y\overline{y}). \end{aligned} \tag{4}$$

This expression is a generalization of others previously proposed in the literature as explained for Machado and Cortínez [16]. In the above expressions ϕ, θ_y and θ_z are measures of the rotations about the shear center axis, $\overline{y}$ and $\overline{z}$ axes, respectively; θ represents the warping variable of the cross-section. Furthermore the superscript 'prime' denotes derivation with respect to the variable x.

The components of the Green's strain tensor which incorporates the large displacement are obtained as explained in [13,16].

3. Variational formulation

Taking into account the adopted assumptions, the principle of virtual work for a composite shell may be expressed in the form:

$$\begin{aligned} &\iint (N_{xx}\delta\varepsilon_{xx}^{(0)} + M_{xx}\delta\kappa_{xx}^{(1)} + N_{xs}\delta\gamma_{xs}^{(0)} + M_{xs}\delta\kappa_{xs}^{(1)} + N_{xn}\delta\gamma_{xn}^{(0)})\,ds\,dx \\ &- \iiint \rho(\ddot{u}_x\delta u_x + \ddot{u}_y\delta u_y + \ddot{u}_z\delta u_z)\,ds\,dn\,dx \\ &- \iint (\overline{q}_x\delta\overline{u}_y + \overline{q}_y\delta\overline{u}_y + \overline{q}_z\delta\overline{u}_z)\,ds\,dx - \iint (\overline{p}_x\delta u_x + \overline{p}_y\delta u_y + \overline{p}_z\delta u_z)|_{x=0}\,ds\,dn \\ &- \iint (\overline{p}_x\delta u_x + \overline{p}_y\delta u_y + \overline{p}_z\delta u_z)|_{x=L}\,ds\,dn - \iiint (\overline{f}_x\delta u_x + \overline{f}_z\delta u_z + \overline{f}_z\delta u_z)\,ds\,dn\,dx = 0, \end{aligned} \tag{5}$$

where N_{xx}, N_{xs}, M_{xx}, M_{xs} and N_{xn} are the shell stress resultants. The beam is subjected to wall surface tractions $\overline{q}_x$, $\overline{q}_y$ and $\overline{q}_z$ specified per unit area of the undeformed middle surface and acting along the x, y and z directions, respectively. Similarly, $\overline{p}_x$, $\overline{p}_y$ and $\overline{p}_z$ are the end tractions per unit area of the undeformed cross-section specified at $x = 0$ and $x = L$, where L is the

undeformed length of the beam. Besides $\bar{f}_x, \bar{f}_y$ and $\bar{f}_z$ are the body forces per unit of volume. Finally, denoting $\bar{u}_x$, $\bar{u}_y$ and $\bar{u}_z$ as displacements at the middle line.

4. Constitutive equations

The constitutive equations of symmetrically balanced laminates may be expressed in the terms of shell stress resultants in the following form [17]:

$$\begin{Bmatrix} N_{xx} \\ N_{xs} \\ N_{xn} \\ M_{xx} \\ M_{xs} \end{Bmatrix} = \begin{bmatrix} \bar{A}_{11} & 0 & 0 & 0 & 0 \\ 0 & \bar{A}_{66} & 0 & 0 & 0 \\ 0 & 0 & \bar{A}_{55}^{(H)} & 0 & 0 \\ 0 & 0 & 0 & \bar{D}_{11} & 0 \\ 0 & 0 & 0 & 0 & \bar{D}_{66} \end{bmatrix} \begin{Bmatrix} \varepsilon_{xx}^{(0)} \\ \gamma_{xs}^{(0)} \\ \gamma_{xn}^{(0)} \\ \kappa_{xx}^{(1)} \\ \kappa_{xs}^{(1)} \end{Bmatrix} \tag{6}$$

with

$$\bar{A}_{11} = A_{11} - \frac{A_{12}^2}{A_{22}}, \quad \bar{A}_{66} = A_{66} - \frac{A_{26}^2}{A_{22}}, \quad \bar{A}_{55}^{(H)} = A_{55}^{(H)} - \frac{\left(A_{45}^{(H)}\right)^2}{A_{44}^{(H)}}, \quad \bar{D}_{11} = D_{11} - \frac{D_{12}^2}{D_{22}}, \quad \bar{D}_{66} = D_{66} - \frac{D_{26}^2}{D_{22}}, \tag{7}$$

where A_{ij}, D_{ij} and $A_{ij}^{(H)}$ are plate stiffness coefficients defined according to the lamination theory presented by Barbero [17]. The coefficient $\bar{D}_{16}$ has been neglected because of its low value for the considered laminate stacking sequence.

5. Principle of virtual work for thin-walled beams

Substituting the kinematics expressions and the constitutive equations Eq. (6) into Eq. (5) and integrating with respect to s, one obtains the one-dimensional expression for the virtual work equation given by:

$$L_M + L_K + L_P = 0, \tag{8}$$

where L_M, L_k and L_p represent the virtual work contributions due to the inertial, internal and external forces, respectively.

$$L_M = \int_0^L \rho \left[A\frac{\partial^2 u_0}{\partial t^2}\delta u_0 + I_z\frac{\partial^2 \theta_z}{\partial t^2}\delta\theta_z + I_y\frac{\partial^2 \theta_y}{\partial t^2}\delta\theta_y + C_w\frac{\partial^2 \theta}{\partial t^2}\delta\theta + A\frac{\partial^2}{\partial t^2}(v - z_0\phi)\delta v + A\frac{\partial^2}{\partial t^2}(w + y_0\phi)\delta w + \frac{\partial^2}{\partial t^2}(-Az_0 v + Ay_0 w + I_s\phi)\delta\phi \right] dx, \tag{9}$$

where A is the cross-sectional area, I_z and I_y are the principal moments of inertia of the cross-section, C_w is the warping constant, I_s is the polar moment with respect to the shear center and ρ is the mean density of the laminate. The expressions of L_K are L_p are the same as presented by the authors in [13] and [16], respectively; in the same way the 1-D beam forces, in terms of the shell forces, have been defined in [16].

5.1. Discrete model

The equations of motion are discretized according to the Galerkin procedure. The independent displacements vector is expressed as a linear combination of given x-function vectors $\mathbf{f}_k(x) = \{f_{k1}(x), f_{k2}(x), f_{k3}(x)\}$ and unknown t-function coefficients $q_k(t)$:

$$\mathbf{u}(x,t) = \sum_{k=1}^{n} q_k(t)\mathbf{f}_k(x). \tag{10}$$

The functions $\mathbf{f}_k(x)$ are chosen as eigenfunctions of the linearized equations and boundary conditions. Since for a generic cross-section even the linear equations are coupled, all the components of $\mathbf{f}_k(x)$ are different from zero. By substituting Eq. (11) into Eq. (8) and vanishing separately terms in δq_k; $3n$ ordinary differential equations of motion follow. The linear natural frequencies of the beam depend on the boundary conditions and the sequence of lamination proposed in the analysis. For specific combinations of system parameters, the lower natural frequencies can be commensurable, leading to internal resonance in the system and nonlinear interaction between the associated modes. We analyze the specific case of three mode interaction corresponding to particular system parameters. Two- and three-to-one internal resonances are considered in this study ($\omega_2 \cong 2\omega_1$ and $\omega_3 \cong 3\omega_1$). Since none of these first three modes is in internal resonance with any other mode of the beam, all other modes except the directly or indirectly excited first, second or third mode decay with time due to the presence of damping and the first three modes will contribute to the long term system response [3]. Therefore, by limiting the expansion Eq. (10) to $n = 3$ terms (e.g. by assuming a group of three modes with similar wave-length), three non-linear equations of the following type are obtained:

$$\ddot{q}_k + \omega_k^2 q_k = \sum_{i=1}^{n}\sum_{j=1}^{n} c_{kij} q_i q_j + \sum_{i=1}^{n}\sum_{j=1}^{n}\sum_{m=1}^{n} c_{kijm} q_i q_j q_m + f_k \quad (k = 1,2,3,\ldots,n), \tag{11}$$

where ω_k is the kth linear frequency, f_k the kth modal force, and c_{kij} and c_{kijm} are coefficients depending on eigenfunctions. In the general case all quadratic and cubic terms appear in each equation of motion.

5.2. Amplitude and phase equations for the discrete model

A simply-supported beam with a monosymmetric cross-section, loaded by a concentrated harmonic force applied to the beam's centroid axis acting along the vertical section is considered, see Fig. 2. Using a three-mode discretization, the non-linear flexural–flexural–torsional oscillations are governed by the following three ordinary differential equations:

$$\begin{aligned}
&\ddot{q}_1 + d_1\dot{q}_1 + \omega_1^2 q_1 = c_1 q_1 q_2 + c_2 q_2 q_3 + c_3 q_1^3 + c_4 q_3^3 + c_5 q_1 q_2^2 + c_6 q_1 q_3^2 + c_7 q_3 q_1^2 + c_8 q_3 q_2^2 + c_{19} P,\\
&\ddot{q}_2 + d_2\dot{q}_2 + \omega_2^2 q_2 = c_9 q_1^2 + c_{10} q_2^2 + c_{11} q_3^2 + c_2 q_1 q_3 + c_{12} q_1 q_2 q_3 + c_{13} q_2^3 + c_5 q_2 q_1^2 + c_{14} q_2 q_3^2,\\
&\ddot{q}_3 + d_3\dot{q}_3 + \omega_3^2 q_3 = c_2 q_1 q_2 + c_{15} q_2 q_3 + c_{16} q_1^3 + c_{17} q_3^3 + c_8 q_1 q_2^2 + c_{18} q_1 q_3^2 + c_6 q_3 q_1^2 + c_{14} q_3 q_2^2 + c_{20} P,
\end{aligned} \tag{12}$$

where q_i is the ith mode amplitude, d_i are the modal damping coefficients and $P(t) = p\, e^{i\Omega t}$ is the load, of frequency Ω assumed to be in primary resonance with the q_1-mode. Moreover, the beam is assumed to be in internal resonance conditions of the kind 2:3:1, so that quadratic, cubic and combination resonances occur.

Eq. (12) is similar to those obtained by Di Egidio et al. [13]; the main difference is in the coefficients c_i because as it is cited in the introduction, their formulation corresponds to a shear undeformable model valid for isotropic beams. The method of multiple time scales is employed to study the non-linear equation (12). Since non-linear terms are quadratic and cubic, a second-order expansion is developed. A small parameter ε is introduced by ordering the linear damping and load amplitude as $d_i = \varepsilon^2 \tilde{d}_i$, $p = \varepsilon^3 \tilde{p}$. Moreover, the displacements q_i are expanded as:

$$q_i(T_0, T_1, T_2, \varepsilon) = \varepsilon q_i^{(0)}(T_0, T_1, T_2, \varepsilon) + \varepsilon^2 q_i^{(1)}(T_0, T_1, T_2, \varepsilon) + \varepsilon^3 q_i^{(2)}(T_0, T_1, T_2, \varepsilon), \tag{13}$$

where, $T_0 = t$, $T_1 = \varepsilon t$, $T_2 = \varepsilon^2 t$. T_0 is a fast scale, on which motions with frequencies of the order of Ω occur, while T_1 and T_2 are the slow scales, on which modulations of the amplitudes and phases take place.

Substituting Eq. (13) into Eq. (12) and equating coefficients of like powers of ε, the following perturbation equations are obtained:

Order ε:

$$D_0^2 q_i^{(0)} + \omega_i^2 q_i^{(0)} = 0 \quad (i = 1,2,3). \tag{14}$$

Orden ε^2:

$$\begin{aligned}
D_0^2 q_1^{(1)} + \omega_1^2 q_1^{(1)} &= -2D_0 D_1 q_1^{(0)} + c_1 q_1^{(0)} q_2^{(0)} + c_2 q_2^{(0)} q_3^{(0)},\\
D_0^2 q_2^{(1)} + \omega_2^2 q_2^{(1)} &= -2D_0 D_1 q_2^{(0)} + c_9 q_1^{(0)^2} + c_{10} q_2^{(0)^2} + c_2 q_1^{(0)} q_3^{(0)} + c_{11} q_3^{(0)^2},\\
D_0^2 q_3^{(1)} + \omega_3^2 q_3^{(1)} &= -2D_0 D_1 q_3^{(0)} + c_2 q_1^{(0)} q_2^{(0)} + c_{15} q_2^{(0)} q_3^{(0)}.
\end{aligned} \tag{15}$$

Orden ε^3:

$$\begin{aligned}
D_0^2 q_1^{(2)} + \omega_1^2 q_1^{(2)} =& -d_1 D_0 q_1^{(0)} - 2D_0 D_1 q_1^{(1)} - D_1^2 q_1^{(0)} - 2D_0 D_2 q_1^{(0)} + c_3 q_1^{(0)^3} + c_1 q_1^{(1)} q_2^{(0)} + c_5 q_1^{(0)} q_2^{(0)^2} + c_1 q_1^{(0)} q_2^{(1)}\\
&+ c_7 q_1^{(0)^2} q_3^{(0)} + c_8 q_2^{(1)^2} q_3^{(0)} + c_2 q_2^{(1)} q_3^{(0)} + c_6 q_1^{(0)} q_3^{(0)^2} + c_4 q_3^{(0)^3} + c_2 q_2^{(0)} q_3^{(1)} + c_{19} p e^{i\Omega T_0},\\
D_0^2 q_2^{(2)} + \omega_2^2 q_2^{(2)} =& -d_2 D_0 q_2^{(0)} - 2D_0 D_1 q_2^{(1)} - D_1^2 q_2^{(0)} - 2D_0 D_2 q_2^{(0)} + 2c_9 q_1^{(0)} q_1^{(1)} + c_5 q_1^{(0)^2} q_2^{(0)} + c_{13} q_2^{(0)^3}\\
&+ 2c_{10} q_2^{(0)} q_2^{(1)} + c_2 q_1^{(1)} q_3^{(0)} + c_{12} q_1^{(0)} q_2^{(0)} q_3^{(0)} + c_{14} q_2^{(0)} q_3^{(0)^2} + c_2 q_1^{(0)} q_3^{(1)} + 2c_{11} q_3^{(0)} q_3^{(1)},\\
D_0^2 q_3^{(2)} + \omega_3^2 q_3^{(2)} =& -d_3 D_0 q_3^{(0)} - 2D_0 D_1 q_3^{(1)} - D_1^2 q_3^{(0)} - 2D_0 D_2 q_3^{(0)} + c_{16} q_1^{(0)^3} + c_2 q_1^{(1)} q_2^{(0)} + c_8 q_1^{(0)} q_2^{(0)^2} + c_2 q_1^{(0)} q_2^{(1)}\\
&+ c_6 q_1^{(0)^2} q_3^{(0)} + c_{14} q_2^{(1)^2} q_3^{(0)} + c_{15} q_2^{(1)} q_3^{(0)} + c_{18} q_1^{(0)} q_3^{(0)^2} + c_{17} q_3^{(0)^3} + c_{15} q_2^{(0)} q_3^{(1)} + c_{20} p e^{i\Omega T_0},
\end{aligned} \tag{16}$$

where

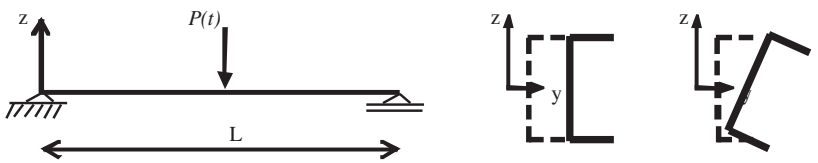

Fig. 2. Simply-supported C-beam and midspan section displacements of the fundamentals eigenfunctions.

$$D_i() = \partial()/\partial(T_i), \quad D_{ij}() = \partial^2()/\partial(T_i)\partial(T_j) \quad (i,j = 0,1,2), \tag{17}$$

and the tilde has been omitted for simplicity.

The solution to the first-order perturbation Eq. (15) is:

$$q_i^{(0)} = A_i(T_1,T_2)e^{\mathrm{i}\omega_i T_0} + c.c. \quad i = 1,2,3, \tag{18}$$

where *c.c.* stands for the complex conjugate of the preceding terms and A_i are the unknown complex-valued functions. In order to investigate the system response under internal and external resonance conditions, three detuning parameters σ_i are introduced:

$$\Omega = \omega_1 + \varepsilon^2\sigma_1, \quad \omega_2 = 2\omega_1 + \varepsilon\sigma_2, \quad \omega_3 = 3\omega_1 + \varepsilon^2\sigma_3. \tag{19}$$

Replacing the first-order solution Eq. (18) into Eq. (15), eliminating the secular terms

$$\begin{aligned} D_1A_1 &= -\frac{\mathrm{i}e^{-\mathrm{i}T_1\sigma_2}(A_2c_1e^{2\mathrm{i}T_1\sigma_2}\overline{A}_1 + A_3c_2e^{\mathrm{i}T_2\sigma_3}\overline{A}_2)}{2\omega_1}, \\ D_1A_2 &= -\frac{\mathrm{i}e^{-\mathrm{i}T_1\sigma_2}(A_1^2c_9 + A_3c_2e^{\mathrm{i}T_2\sigma_3}\overline{A}_1)}{2\omega_2}, \\ D_1A_3 &= -\frac{\mathrm{i}A_1A_2c_2e^{\mathrm{i}T_1\sigma_2-\mathrm{i}T_2\sigma_3}}{2\omega_3}. \end{aligned} \tag{20}$$

The solution considering the quadratic terms are the same as presented by the authors in [13]. Finally, substituting the solution into the ε^3-order perturbation equations Eq. (16), eliminating again the secular terms and taking into account Eq. (19), leads to

$$\begin{aligned} D_2A_1 &= \frac{1}{2\mathrm{i}\omega_1}\left(c_{19}pe^{\mathrm{i}T_2\sigma_1} - \mathrm{i}A_1d_1\omega_1 + A_1^2b_1\overline{A}_1 - \frac{A_2c_1e^{\mathrm{i}T_1\sigma_2}\sigma_2\overline{A}_1}{2\omega_1} + A_3b_2e^{\mathrm{i}T_2\sigma_3}\overline{A}_1^2 + A_1A_2b_3\overline{A}_2 + A_1A_3b_5\overline{A}_3\right. \\ &\quad \left. + \frac{A_3c_2e^{\mathrm{i}(T_2\sigma_3-T_1\sigma_2)}\sigma_2\overline{A}_2}{2\omega_1} + A_2^2b_4e^{\mathrm{i}(2T_1\sigma_2-T_2\sigma_3)}\overline{A}_3\right), \\ D_2A_2 &= \frac{1}{2\mathrm{i}\omega_2}\left(\frac{A_1^2c_9e^{-\mathrm{i}T_1\sigma_2}\sigma_2}{2\omega_2} - \mathrm{i}A_2d_2\omega_2 + A_1A_2b_6\overline{A}_1 + A_1A_3b_9e^{\mathrm{i}(T_2\sigma_3-2T_1\sigma_2)}\overline{A}_2 + A_2A_3b_8\overline{A}_3 + A_2^2b_7\overline{A}_2 + \frac{A_3c_2e^{\mathrm{i}(T_2\sigma_3-T_1\sigma_2)}\sigma_2\overline{A}_1}{2\omega_2}\right), \\ D_2A_3 &= \frac{1}{2\mathrm{i}\omega_3}\left(\frac{A_1A_2c_2e^{\mathrm{i}(T_1\sigma_2-T_2\sigma_3)}\sigma_2}{2\omega_3} - \mathrm{i}A_3d_3\omega_3 + A_1^3b_{10}e^{-\mathrm{i}T_2\sigma_3} + A_1A_3b_{12}\overline{A}_1 + A_3^2b_{14}\overline{A}_3 + A_2A_3b_{13}\overline{A}_2 + A_2^2b_{11}e^{\mathrm{i}(2T_1\sigma_2-T_2\sigma_3)}\overline{A}_1\right), \end{aligned} \tag{21}$$

where the b_j values are presented in Appendix A.

Finally, using a reconstitution method [15] to return to true time t, see Eq. (22), the amplitude and phase equations obtained are the same presented by the authors in [13].

$$A_k' = \varepsilon D_1A_k + \varepsilon^2D_2A_k + \cdots. \tag{22}$$

6. Numerical results

Non-linear coupling and resonant motions are investigated for a beam simply supported. In the numerical investigation the following geometrical and material characteristic are used: L = 6 m, h = 0.6 m, b = 0.6 m, e = 0.03 m. The analyzed material is graphite-epoxy whose properties are E_1 = 144 GPa, E_2 = 9.65 GPa, G_{12} = 4.14 GPa, G_{13} = 4.14 GPa, G_{23} = 3.45 GPa, ν_{12} = 0.3, ν_{13} = 0.3, ν_{23} = 0.5, for a sequence of lamination {0/0/0/0}.

The solution of the linear free dynamic problem furnishes the following first three eigenvalues:

$$\omega_1 = 213.86 \text{ rad/s}, \quad \omega_2 = 444.36 \text{ rad/s}, \quad \omega_3 = 666.85 \text{ rad/s}.$$

The coefficients of the discretized equations of motion Eq. (12) are listed in Table 1.

Table 1
Coefficients of the non-dimensional discretized equations of motion.

c_1	c_2	c_3	c_4	c_5	c_6	c_7
23134.1	−38059.0	−12549.1	51358.0	−2057.39	−93052.5	58212.7
c_8	c_9	c_{10}	c_{11}	c_{12}	c_{13}	c_{14}
3375.58	11569.2	322.56	31345.8	6752.41	−0.61	0.0
c_{15}	c_{16}	c_{17}	c_{18}	c_{19}	c_{20}	
62660.6	19398.2	−87918.5	154026.0	−0.00517	−0.00651	

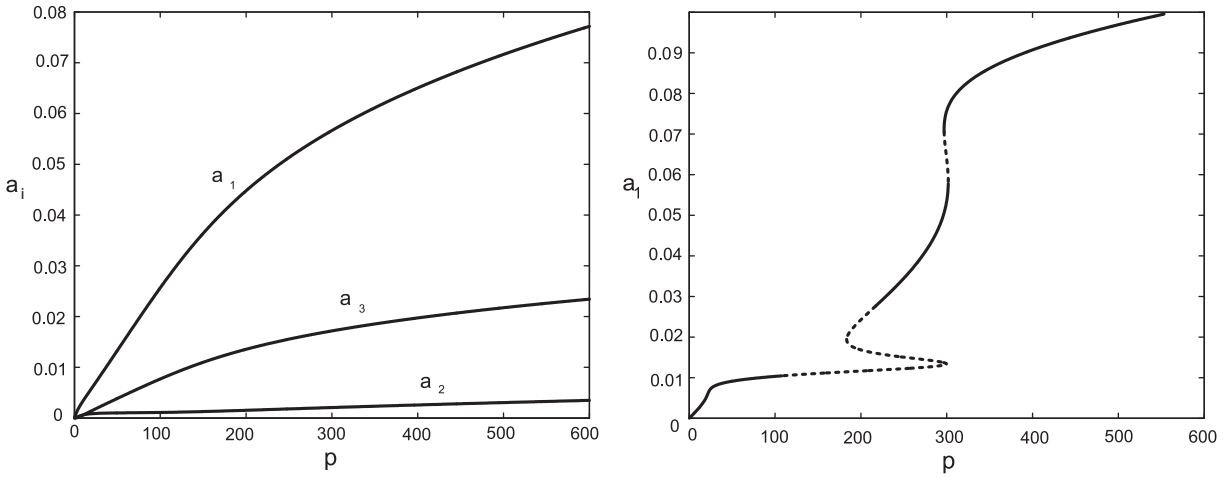

Fig. 3. Amplitude-load curves: (a) perfect external resonance $\sigma_1 = 0$; and (b) external detuning parameter $\sigma_1 = 0.1$. Thick line: stable solutions; dashed line: unstable solutions.

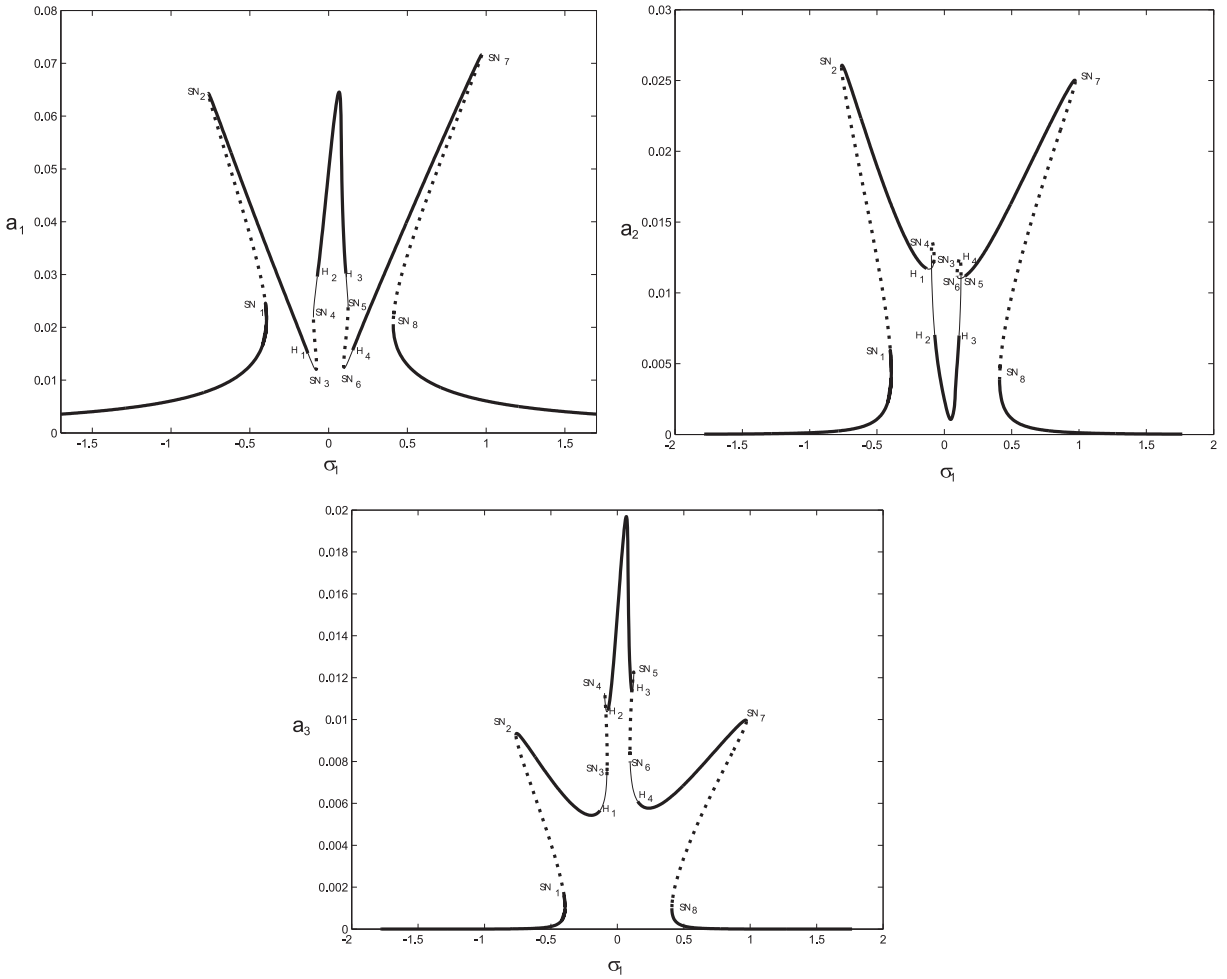

Fig. 4. Frequency–response curves for: (a) first, (b) second and (c) third modes, when $p = 250$, $\sigma_2 = \sigma_3 = 0.04$ and $d_i = 0.1$. Solid (dotted) lines denote stable (unstable) equilibrium solutions and thin solid lines denote unstable foci.

6.1. Steady-state motions and stability

The equilibrium solutions correspond to periodic motions of the beam. Steady-state solutions are determined by zeroing $p_i' = q_i' = 0$ the right-hand members of the modulation equations [13] and solving the non-linear system. Stability analysis is then performed by analyzing the eigenvalues of the Jacobian matrix of the non-linear equations calculated at the fixed points. Amplitude-load curves are reported in Fig. 3(a) and (b), for external forces in a perfect resonance condition ($\sigma_1 = 0$) and for a small value of the external detuning parameter $\sigma_1 = 0.1$, respectively, considering damping $d_1 = d_2 = d_3 = 0.1$ and internal detuning parameters $\sigma_2 = \sigma_3 = 0.04$. The amplitudes a_1, a_2 and a_3 are obtained by means of the following expression:

$$a_i = \sqrt{p_i^2 + q_i^2} \quad i = 1, 2, 3. \tag{23}$$

In the case of $\sigma_1 = 0.1$ (Fig. 3(b)), the modal solution branch alternatively loses and regains stability due to the presence of some saddle-nodes and Hopf bifurcations. In spite of that only the amplitude a_1 is presented in Fig. 3(b), the same behavior is obtained for the other amplitudes.

The frequency–response curves are show in Fig. 4(a)–(c), for an internal and external resonance condition. The modal amplitude a_i curves are obtained in function of the external detuning parameter σ_1. In this case, the forcing amplitude is $p = 250$, modal damping $d_1 = d_2 = d_3 = 0.1$ and internal detuning parameters $\sigma_2 = \sigma_3 = 0.04$. In this way, near to $\sigma_1 = 0.1$ the dynamic behavior will be complex as can be observed from Fig. 3(b). In Fig. 4, solid (dotted) lines denote stable (unstable) equilibrium solutions and thin solid lines denote unstable foci.

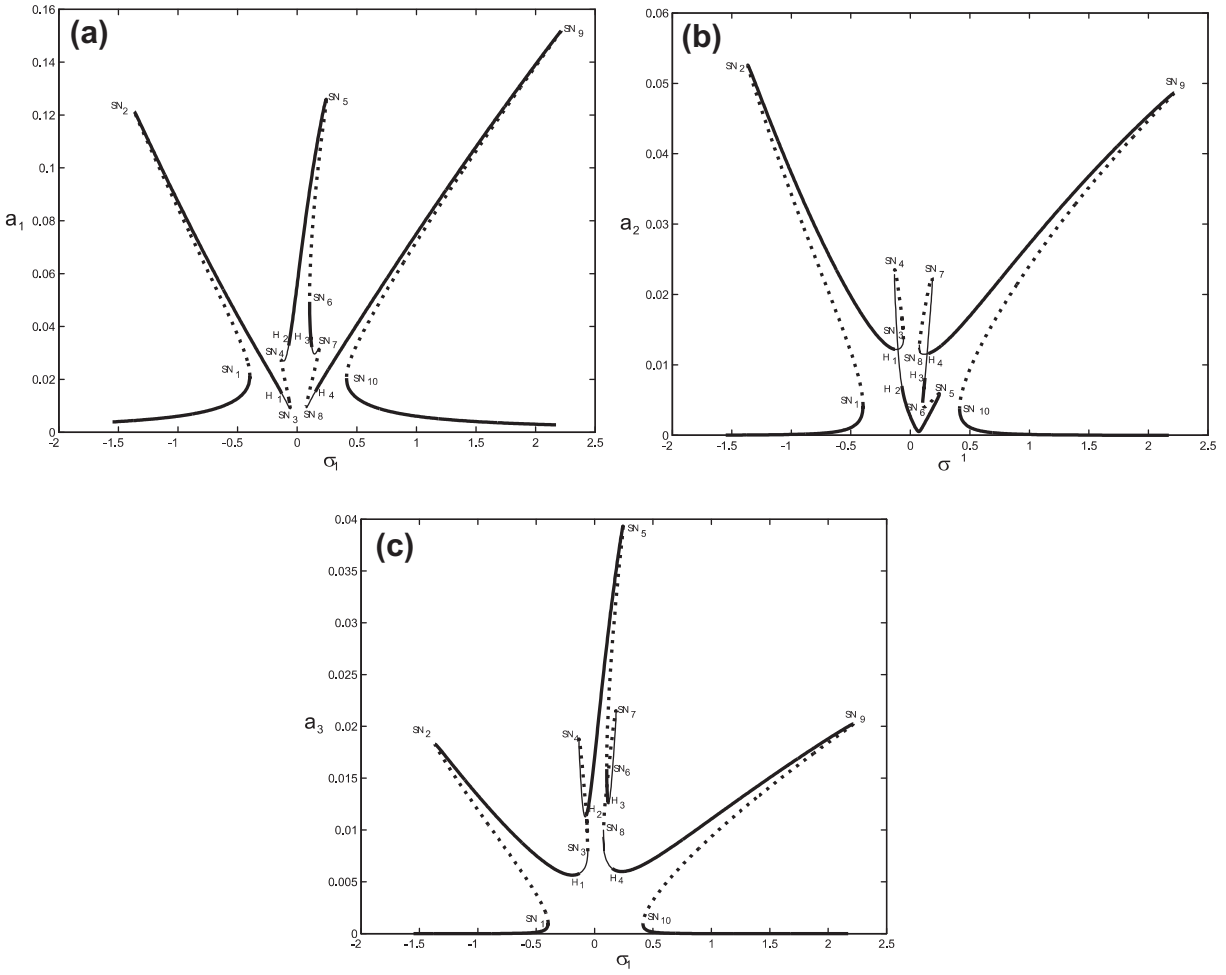

Fig. 5. Frequency–response curves for $d_i = 0.05$: (a) first, (b) second and (c) third modes, when $p = 250$ and $\sigma_2 = \sigma_3 = 0.04$. Solid (dotted) lines denote stable (unstable) equilibrium solutions and thin solid lines denote unstable foci.

The response curves exhibit a complex behavior due to saddle-node bifurcations (where one of the corresponding eigenvalues crosses the imaginary axis along the real axis from the left- to the right-half plane) and Hopf bifurcations (where one pair of complex conjugate eigenvalues crosses the imaginary axis transversely from the left to the right-half plane). As σ_1 increases from a small value, the solution increases in amplitude and is stable until a saddle-node bifurcation occurs $\sigma_1 = -0.3938$ (SN_1). Then, the response jumps to another branches of stable equilibrium solutions (jump effect), depending on the initial conditions. Increasing σ_1, the amplitude decreases until the stable equilibrium solution loses stability via a Hopf bifurcation at H_1 ($\sigma_1 = -0.1307$). Then, the solution is unstable happening two saddle-node bifurcations SN_3 and SN_4 ($\sigma_1 = -0.0763$ and $\sigma_1 = -0.0961$) and regains its stability via a reverse Hopf bifurcation at H_2 ($\sigma_1 = -0.0724$). Then, an approximated symmetric solution is observed for σ_1 larger than the perfect external resonant condition. Therefore, the solution loses stability via a Hopf bifurcation H_3 ($\sigma_1 = 0.1094$), and regains its stability via a reverse Hopf bifurcation at H_4 ($\sigma_1 = 0.1530$), happening two saddle-node bifurcations SN_5 and SN_6, ($\sigma_1 = 0.1238$ and $\sigma_1 = 0.0946$). The stable solution grows again in amplitude until arriving to a saddle-node bifurcation SN_7 ($\sigma_1 = 0.9718$), resulting in a jump of the response to another branches of solutions. The new stable branch is left bounded by a saddle-node bifurcation SN_8 ($\sigma_1 = 0.4102$). On the other hand, comparing the three modal amplitude a_i curves, the highest values correspond to the first mode which is directly excited by the external load.

In Fig. 5 we show the influence of damping when the modal damping value is reduced to $d_i = 0.05$, conserving the same forcing amplitude and internal detuning parameter values. The frequency–response curves are similar to the previous case, and as expected the modal amplitudes result to be larger. It can be seen in the first mode that the central peak is slightly

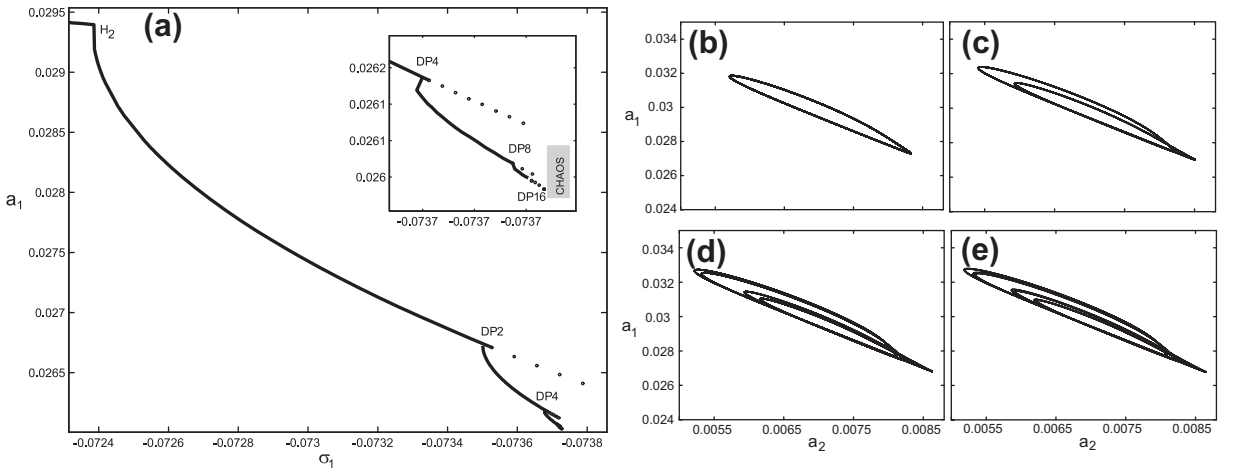

Fig. 6. (a) Schematic of the dynamic solutions found on one branch for the first mode. (——) Stable limit cycle, (o o o) unstable limit cycle, DPn = nth period-doubling bifurcation. Two-dimensional projections of the phase portraits onto the a_1–a_2 plane, (b) $\sigma_1 = -0.0734455$, (c) $\sigma_1 = -0.07358$, (d) $\sigma_1 = -0.073695$, and (e) $\sigma_1 = -0.073715$.

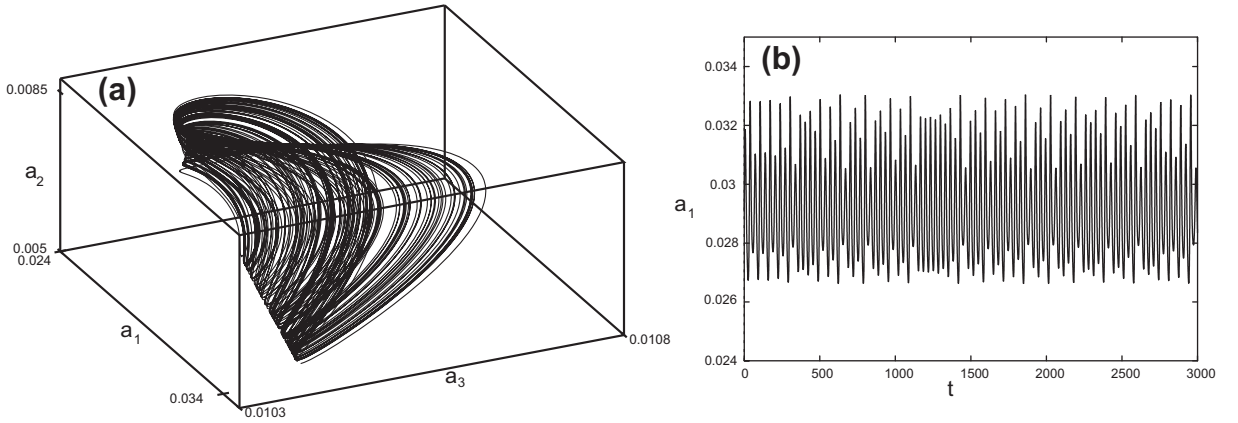

Fig. 7. Attractor chaotic found at $\sigma_1 = -0.0737899$. (a) Three-dimensional projection of the phase portrait onto the a_1–a_2–a_3 space, and (d) time history.

curved to the right ($\sigma_1 \approx 0$), giving rise to a new unstable branch bounded by two saddle-node bifurcations (SN_5, $\sigma_1 = 0.2437$ and SN_6, $\sigma_1 = 0.1035$).

6.2. Dynamic solutions

According to the Hopf bifurcation theorem, small limit cycles are born as a result of the Hopf bifurcation. It is very complex to reduce our six-dimensional system [13] to obtain the normal form of the modulation equations in the vicinity of the bifurcations. Therefore, the software AUTO [18] is used to obtain dynamic solutions that emerge from the Hopf bifurcations. The Hopf bifurcation is supercritical or subcritical depending on whether the born limit cycle is stable or unstable, respectively. Cycle-limit of the modulation equations correspond to aperiodic responses of the beam. In the previous example ($d_3 = 0.1$, $\sigma_2 = \sigma_3 = 0.04$ and $p = 250$), there are four Hopf bifurcations. Where H_1 ($\sigma_1 = -0.1307$) and H_4 ($\sigma_1 = 0.1530$) represent subcritical Hopf bifurcation, while H_2 ($\sigma_1 = -0.0724$) and H_3 ($\sigma_1 = 0.1094$) correspond to supercritical Hopf bifurcation. As σ_1 increases, a small limit cycle born as a result of the supercritical Hopf bifurcation point H_2, see Fig. 6(a). The period-one limit cycle (Fig. 6(b)) grows and deforms and remains stable until another period-doubling bifurcation occurs DP_2 ($\sigma_1 = -0.07353$). Then it undergoes a sequence of period-doubling bifurcations DP_4 ($\sigma_1 = -0.07368$), DP_8 ($\sigma_1 = -0.07371$), DP_{16} ($\sigma_1 = -0.073721$), culminating in a chaotic attractor as shown in Fig. 7. In Fig. 6(c)–(e), two-dimensional projections of the phase portraits onto the a_1–a_2 plane at various pre and post-period-doubling bifurcation points are shown.

7. Summary and conclusions

In this paper a geometrically non-linear theory for thin-walled composite beams is used to present the nonlinear dynamic response of a thin-walled composite beam. The theory is formulated in the context of large displacements and rotations, adopting a shear deformable displacement field and valid for bisymmetric cross-sections either open or closed. The internal resonance is present in the beam dynamic behavior. With the method of multiple scales six first-order nonlinear ordinary-differential equations describing the modulation of the amplitudes and phases were obtained and numerically analyzed. The resonant behavior is illustrated by frequency–response and amplitude-load curves for a sequence of lamination of {0/0/0/0}. Due to the coupling existing, the composite thin-walled beam exhibit a complex dynamic behavior. The frequency–response curves are characterized by saddle-node and Hopf bifurcations and multiple jumps effects. Supercritical and subcritical Hopf bifurcations of the three-mode equilibrium solutions are found. The limit cycle solutions which born from the Hopf bifurcation may undergo a sequence of period-doubling bifurcations, culminating in an chaotic attractor. There are new periodic solutions in the frequency–response curves when the damping value decreases.

Acknowledgements

The present study was sponsored by Secretaría de Ciencia y Tecnología, Universidad Tecnológica Nacional, and by CONICET.

Appendix A.

The coefficients used in the Eq. (21) are:

$$
\begin{aligned}
&b_1 = 3c_3 + 2c_1c_9K_8 + \frac{c_1c_9}{4\omega_1\omega_2}, \quad b_2 = c_7 + \frac{c_1c_2}{4\omega_1\omega_2} - \frac{c_2c_9}{4\omega_1\omega_2},\\
&b_3 = 2c_5 + c_1^2K_2 + c_2^2K_4 + 2c_1c_{10}K_8 - \frac{c_1^2}{4\omega_1^2} + \frac{c_2^2}{4\omega_1\omega_3}, \quad b_4 = c_8 - c_{15}c_2K_5 - \frac{c_{10}c_2K_8}{3} - \frac{c_1c_2}{4\omega_1^2},\\
&b_5 = 2c_6 - c_2^2K_6 + 2c_1c_{11}K_8 - \frac{c_2^2}{4\omega_1\omega_2}, \quad b_6 = 2c_5 + 2c_1c_9K_2 + c_2^2K_4 + 4c_{10}c_9K_8 + \frac{c_1c_9}{2\omega_1\omega_2} + \frac{c_2^2}{4\omega_2\omega_3},\\
&b_7 = 3c_{13} + \frac{10c_{10}^2K_8}{3}, \quad b_8 = 2c_{14} - c_2^2K_1 - 2c_{11}c_{15}(K_3 + K_5) + 4c_{10}c_{11}K_8 - \frac{c_2^2}{4\omega_1\omega_2},\\
&b_9 = c_{12} + 2c_{11}c_2K_4 - c_{15}c_2K_5 - 2c_{10}c_2K_6 - \frac{c_1c_2}{4\omega_1\omega_2} + \frac{c_2c_9}{2\omega_1\omega_2}, \quad b_{10} = c_{16} + \frac{c_2c_9}{4\omega_2\omega_3},\\
&b_{11} = c_8 + c_{15}c_2K_4 - \frac{c_{10}c_2K_8}{3} + \frac{c_1c_2}{4\omega_1\omega_3}, \quad b_{12} = 2c_6 - c_2^2K_6 + 2c_{15}c_9K_8 + \frac{c_2^2}{4\omega_2\omega_3},\\
&b_{13} = 2c_{14} - c_2^2K_1 - c_{15}^2K_3 - c_{15}^2K_5 + 2c_{10}c_{15}K_8 + \frac{c_2^2}{4\omega_1\omega_3}, \quad b_{14} = 3c_{17} + c_{11}c_{15}K_7 + 2c_{11}c_{15}K_8,
\end{aligned}
\tag{A.1}
$$

where

$$K_1 = \frac{1}{(\omega_2+\omega_3)^2-\omega_1^2}, \quad K_2 = -\frac{1}{2\omega_1\omega_2+\omega_2^2}, \quad K_3 = \frac{1}{2\omega_2\omega_3+\omega_2^2},$$
$$K_4 = \frac{1}{\omega_3^2-(\omega_1-\omega_2)^2}, \quad K_5 = \frac{1}{\omega_2^2-2\omega_2\omega_3}, \quad K_6 = \frac{1}{(\omega_1+\omega_3)^2-\omega_2^2}, \tag{A.2}$$
$$K_7 = \frac{1}{\omega_2^2-4\omega_3^2}, \quad K_8 = \frac{1}{\omega_2^2}.$$

References

[1] A.H. Nayfeh, D.T. Mook, Nonlinear Oscillations, Wiley, New York, 1979.
[2] A.H. Nayfeh, B. Balachandran, Modal interactions in dynamical and structural systems, Appl. Mech. Rev. 42 (1989) 175–2011.
[3] A.H. Nayfeh, Nonlinear Interactions, Wiley, New York, 1996.
[4] M.R.M. Crespo da Silva, C.C. Glynn, Nonlinear flexural–flexural–torsional dynamics of inextensional beams. I. Equations of motion, J. Struct. Mech. 6 (1978) 437–448.
[5] M.R.M. Crespo da Silva, C.C. Glynn, Nonlinear flexural-flexural-torsional dynamics of inextensional beams. II. Forced motions, J. Struct. Mech. 6 (1978) 449–461.
[6] A. Luongo, G. Rega, F. Vestroni, Non resonant non-planar free motions of inextensional non-compact beams, J. Sound Vib. 134 (1989) 73–86.
[7] M.R.M. Crespo da Silva, C.L. Zaretzky, Nonlinear flexural–flexural–torsional interactions in beams including the effect of torsional dynamics. I: primary resonance, Nonlinear Dynam. 5 (1994) 3–23.
[8] J.R. Fonseca, P. Ribeiro, Beam p-version finite element for geometrically nonlinear vibrations in space, Comput. Methods Appl. Mech. Eng. 195 (2006) 905–924.
[9] R. Lopes Alonso, P. Ribeiro, Flexural and torsional non-linear free vibrations of beams using a p-version finite element, Comput. Struct. 86 (2008) 1189–1197.
[10] S. Stoyko, P. Ribeiro, Nonlinear forced vibrations and static deformations of 3D beams with rectangular cross section: the influence of warping, shear deformation and longitudinal displacements, Int. J. Mech. Sci. 52 (2010) 1505–1521.
[11] A. Di Egidio, A. Luong, F. Vestroni, A non-linear model for the dynamics of open cross-section thin-walled beams – Part I: formulation, Int. J. Nonlinear Mech. 38 (2003) 1067–1081.
[12] A. Di Egidio, A. Luongo, F. Vestroni, A non-linear model for the dynamics of open cross-section thin-walled beams – Part II: forced motion, Int. J. Nonlinear Mech. 38 (2003) 1083–1094.
[13] S.P. Machado, C.M. Saravia, Shear-deformable thin-walled composite beams in internal and external resonance, Comput. Struct. 97 (2013) 30–39.
[14] A.H. Nayfeh, Perturbation Methods, Pure & Applied Mathematics-A, Wiley, New York, 1973.
[15] A.H. Nayfeh, B. Balachandran, Applied Nonlinear Dynamics: Analytical Computational and Experimental Methods, Wiley-Interscience, 1995.
[16] S.P. Machado, V.H. Cortínez, Non-Linear model for stability of thin walled composite beams with shear deformation, Thin Wall Struct. 43 (2005) 1615–1645.
[17] E. Barbero, Introduction to Composite Material Design, Taylor and Francis Inc., 1999.
[18] E.J. Doedel, AUTO97 continuation and bifurcation software for ordinary differential equations, Available FTP.CS.CONCORDIA.CA, directory PUB/DOEDEL/AUTO, 1997.